Climate Dynamics (2004) 22: 527–538
DOI 10.1007/s00382-004-0395-z

V. Romanova · M. Prange · G. Lohmann

Stability of the glacial thermohaline circulation and its dependence on the background hydrological cycle

Received: 10 April 2003 / Accepted: 29 December 2003 / Published online: 24 March 2004

Abstract Different reconstructions of glacial sea-surface temperatures (SST) are used to force a hybrid coupled atmosphere–ocean model. The resulting glacial states differ in global salinity and temperature distributions, and consequently in the strength of the thermohaline circulation. Stability analysis of the Atlantic Ocean circulation, by means of freshwater-flux hysteresis maps, reveals mono-stability for each glacial background state, which appears to be a robust feature of the glacial ocean. We show that this behaviour is directly linked to the hydrological cycle. A monotonic relation between the freshwater input necessary for reaching the off-mode and the hydrological budget in the Atlantic catchment area, accounts for the sensitivity of the ocean's circulation. The most sensitive part of the hydrological balance appears to be in the tropical and subtropical regions suggesting that the 'Achilles heel' of the global conveyor belt circulation is not restricted to the northern North Atlantic where convection occurs.

1 Introduction

Transporting heat over large distances, the thermohaline circulation (THC) plays a pivotal role in the climate system. Geological records from the Last Glaciation indicate that greater abundances of ice-rafted debris in the North Atlantic (Heinrich Events) were associated with global-scale climatic changes (Broecker and Hemming 2001), probably resulting from a THC slowdown (Boyle and Keigwin 1987; Clark et al. 2002). The concept of THC fluctuations with global impact has motivated a large number of researchers to study the sensitivity of the circulation to North Atlantic meltwater inflow, utilizing numerical climate models (e.g. Bryan 1986; Maier-Reimer and Mikolajewicz 1989; Stocker and Wright 1991; Mikolajewicz and Maier-Reimer 1994; Manabe and Stouffer 1995; Rahmstorf 1995; Lohmann et al. 1996a; Rahmstorf 1996; Fanning and Weaver 1997; Schiller et al. 1997; Rind et al. 2001). In many of these models, the THC possesses multiple equilibria, and transitions from one mode of operation to another can be triggered by a sufficiently strong freshwater perturbation. Consequently, a short-term meltwater influx can have a persistent effect on the THC by inducing a transition from a mode with intense North Atlantic Deep Water (NADW) formation to a mode with weak or ceased convective activity.

In model experiments, meltwater perturbations were usually applied to present-day states of the THC. The suitability of such experiments for *glacial* conditions has been challenged by results from box models, suggesting that the weaker overturning circulation of the ice age was more vulnerable than the modern one (Lohmann et al. 1996b; Prange et al. 1997). A recent study by Ganopolski and Rahmstorf (2001) provides a new perspective on the stability properties of glacial climate. Utilizing an earth system model of intermediate complexity, the authors suggested that the glacial THC possesses only one equilibrium. This mono-stable behaviour of the THC may explain the conveyor's recovery after a meltwater-induced shutdown associated with a Heinrich Event. The results of Ganopolski and Rahmstorf (2001) were corroborated by Prange et al. (2002), who demonstrated the mono-stability of the THC in a hybrid-coupled model with a three-dimensional ocean under glacial conditions. In their modelling approach, the authors used CLIMAP (1981) surface

V. Romanova (✉) · M. Prange · G. Lohmann
Geoscience Department,
University of Bremen,
Klagenfurterstr.,
28334 Bremen, Germany
E-mail: vanya@palmod.uni-bremen.de

M. Prange · G. Lohmann
DFG Research Center Ocean Margins (RCOM),
University of Bremen,
28334 Bremen, Germany

temperatures with an additional cooling in the tropics to force the atmospheric circulation (Lohmann and Lorenz 2000) as background climate state. This reconstruction is characterized by an extensive North Atlantic sea ice cover: the Nordic Seas are ice-covered the whole year round, and the winter ice cover advances southward to almost 45°N. More recent reconstructions, however, provide evidence for a substantially reduced ice coverage with vast ice-free areas in the Nordic Seas during summer (Weinelt et al. 1996; Paul and Schäfer-Neth 2003).

Extending the work of Prange et al. (2002), this study applies the surface temperature reconstructions of Weinelt et al. (1996) and GLAMAP 2000 (Paul and Schäfer-Neth 2003) in a hybrid-coupled climate model. We shall examine the effects of different glacial sea surface temperature fields on the hydrologic cycle, salinity distributions and the oceanic circulation. In particular, we focus on the stability of the glacial THC and its dependence on the background hydrological cycle.

The work is organized as follows: in Sect. 2, the model and experimental set-up is described. The results are presented in the third section and they are discussed in Sect. 4. Conclusions are drawn in the fifth section.

2 Model description and experimental set-up

2.1 Atmospheric model

We use the three-dimensional atmospheric general circulation model (AGCM) ECHAM3/T42 (Roeckner et al. 1992). It is based on the primitive equations and includes radiation and hydrological cycle. It has 19 levels and a resolution of 128 × 64 points on a Gaussian grid. The forcing is given by insolation, following the astronomical theory of Milankovic and CO_2 concentration. The orbital parameters for 21,000 years BP are taken to calculate the insolation pattern, which remains unchanged during the experiments. The CO_2 concentration is fixed to 200 ppm for the glacial simulations and to 345 ppm for the control run (Lohmann and Lorenz 2000). The bottom boundary conditions are given by the Earth's orography, including ice sheets (Peltier 1994), albedo, sea-ice cover and sea surface temperatures. The last two parameters are taken from three different reconstruction sets. As yet, the model has no dynamic ice sheets. The model output comprises the monthly averaged surface freshwater fluxes, surface air temperatures and wind stresses. The model is run for 15 years of model integration and averaged years are constructed from the last 10 years of the simulations.

2.2 Oceanic model

The ocean model is based on the LSG ocean circulation model. It integrates the primitive equations, including all terms except the nonlinear advection of momentum, using a time step of 1 month (Maier-Reimer et al. 1993). It has a horizontal resolution of 3.5° × 3.5° and 11 vertical levels on a semi-staggered grid type 'E'. Parametrization of the density is given by the UNESCO formula. A new numerical scheme for the advection of temperature and salinity has been implemented (Schäfer-Neth and Paul 2001; Prange et al. 2003). It uses a predictor-corrector method, as the predictor step is centred differences and the corrector step is a third-order QUICK scheme (Leonard 1979). The advantage of this scheme is the reduced numerical diffusion in comparison with the previously used upstream scheme. The vertical diffusivity is prescribed ranging from 0.6 $cm^2\ s^{-1}$ at the surface up to 1.3 $cm^2\ s^{-1}$ in the abyssal ocean. The sea level is reduced by 120 m, accounting for the water stored in the land ice, thus the Bering Strait is closed.

2.3 Hybrid coupling

The monthly averaged surface freshwater fluxes, surface air temperatures and wind stresses calculated with the AGCM are applied to the upper boundary conditions of the OGCM. The coupling is made by including a run-off scheme. The boundary heat flux Q at the ocean surface is formulated as suggested by Rahmstorf and Willebrand (1995):

$$Q = (\lambda_1 - \lambda_2 \nabla^2)(T_a - T_s)$$

allowing for scale-selective damping of temperature anomalies. Here, $T_a$is the prescribed air temperature, and T_s denotes the ocean surface temperature (λ_1 and λ_1 are chosen to be 15 $Wm^{-2}\ K^{-1}$ and $2*10^{12}$ $W\ K^{-1}$). In the model, sea surface salinity (SSS) can freely evolve. When the grid cells are covered by sea ice the surface temperatures are set to the freezing point.

An extensive parameter study of this hybrid-coupled model approach has been carried out by Prange et al. (2003). It has been shown that this model approach is able to simulate variable sea surface temperatures and salinities and it has been applied to deglaciation scenarios (Knorr and Lohmann 2003; Rühlemann et al. 2004; Prange et al. 2004). The model set-up neglects feedbacks connected with atmospheric dynamics, vegetation and cryosphere.

2.4 Experimental set-up

The control run is forced with present-day SSTs used in AMIP (Atmospheric Model Intercomparison Project) and is discussed in Prange et al. (2003). For the glacial we use three different SST and sea-ice reconstruction data sets. Experiment **C**, the reference experiment, employs CLIMAP (1981) SST and sea ice. This reconstruction uses samples for a time interval between 24 and 14 ^{14}C ka BP, in which a climatic stability is assumed (Mix et al. 2001). An additional tropical cooling of 3 °C is applied in the tropics. It has been shown that this provides for a consistency with terrestrial and marine proxy data during the Last Glacial Maximum (LGM) (Farrera et al. 1999; Lohmann and Lorenz 2000). The second experiment **W** is forced with SST reconstructions of Weinelt et al. (1996) for the Nordic Seas, combined with the CLIMAP data set (Schäfer-Neth and Paul 2001). This reconstruction assumes LGM as a period of climatic stability and minimum meltwater flux for the time interval between 18 and 15 ^{14}C ka BP. The data set shows seasonally ice-free conditions in most parts of the Nordic Seas (see Fig. 3b) along with higher summer SST than in the CLIMAP (1981) reconstruction. A recent reconstruction, GLAMAP 2000 (German Glacial Atlantic Ocean Mapping Project), comprises the North, Central and South Atlantic Ocean using joint definitions of the LGM time slice as the overlap of the Last Isotope Maximum (18-15 ^{14}C ka BP) and the EPILOG Level-1 (19-16 ^{14}C ka BP) time span, sedimentation rates and resolution (Paul and Schäfer-Neth 2003). A detailed description of the choice of the LGM slice and age control is given in Sarnthein et al. (2003). It uses 275 sediment cores and the SST estimates are based on a new set of more than 1000 reference samples of planktonic foraminifera, radiolarians and diatoms, and on improved transfer-function techniques. The winter sea ice in the GLAMAP 2000 reconstruction is similar to the CLIMAP summer sea ice boundary and the Nordic Seas are ice-free during the summer months (see Fig. 4). The whole year round, the SSTs are significantly higher in the North Atlantic compared with the CLIMAP reconstruction. The summer SSTs are considerably higher around Newfoundland and the Nordic Seas. The simulation using the SSTs provided by GLAMAP 2000 is indicated by the abbreviation **G**. The experiments described above are called 'glacial experiments' hereafter.

3 Results

3.1 Glacial surface air temperature anomalies

Using different forcings, the AGCM simulates three different states of the glacial climate. Figure 1 shows the North Atlantic anomalous near-surface air temperature relative to present-day temperatures for the LGM. A particularly strong cooling in high northern latitudes is found in all cases, caused by the increase of the albedo due to the vast ice-sheets over the continents (Peltier 1994), the expanded sea-ice cover and advection of cold air from the ice sheets. Experiment **C** yields a temperature reduction of more than 10 °C over northern Europe, Greenland and the Nordic Seas, which are ice-covered the whole year round (Fig. 1). Experiments **W**and **G** show the strongest cooling over the continents and smaller temperature anomalies over the Nordic Seas due to the heat exchange between the atmosphere and the surface waters. The strongest cooling in the tropics (of 5 °C) occurs in experiment **C**.

3.2 The oceanic equilibrium states

The oceanic equilibrium states are obtained after 5500 years of model integration, starting from the present-day hydrography with a global salinity increase of 1 psu. The results are shown as a 40 year mean. The results for different oceanic equilibrium states are displayed in Figs. 2, 3, and 4, respectively. The sea ice conditions strongly vary for the different cases. In the Figs. 2a, 3a and 4a, the grey fill shows the winter sea-ice cover and in Figs. 2b, 3b and 4b the summer sea-ice cover. The summer sea-ice margin in experiment **C** is situated south of Iceland at about 60°N, while in **W** and **G** it is north of Iceland, and the Labrador Sea is partly ice-free.

The anomalous salinity field, averaged over the top 150 m for experiment **C** is shown in Fig. 2a relative to present-day. Taking the global salinity elevation of 1 psu into account, the glacial upper ocean appears relatively fresh. The salinity of the surface waters decreases gradually from the tropics to the north recharging 45°N and further. A salty tongue of 35.0 psu spreads southward of Iceland up to the summer sea ice margin (not shown). The salinity differences of **W** and **G** relative to **C** are shown in Figs. 3a and 4a. A slight salinity increase occurs at 60°N in the southern vicinities of Iceland, favouring NADW formation in these regions. Experiment **G** shows positive salinity anomalies (around +1 psu) in the Northern Hemisphere and negative anomalies (around –1 psu) in the Southern Hemisphere in the Atlantic relative to experiment **C**. This enhanced north-south salinity contrast is not representative for experiment **W**, where the anomalies are positive in the whole Atlantic. In the South Pacific we find a highly saline subtropical gyre (maximum salinity

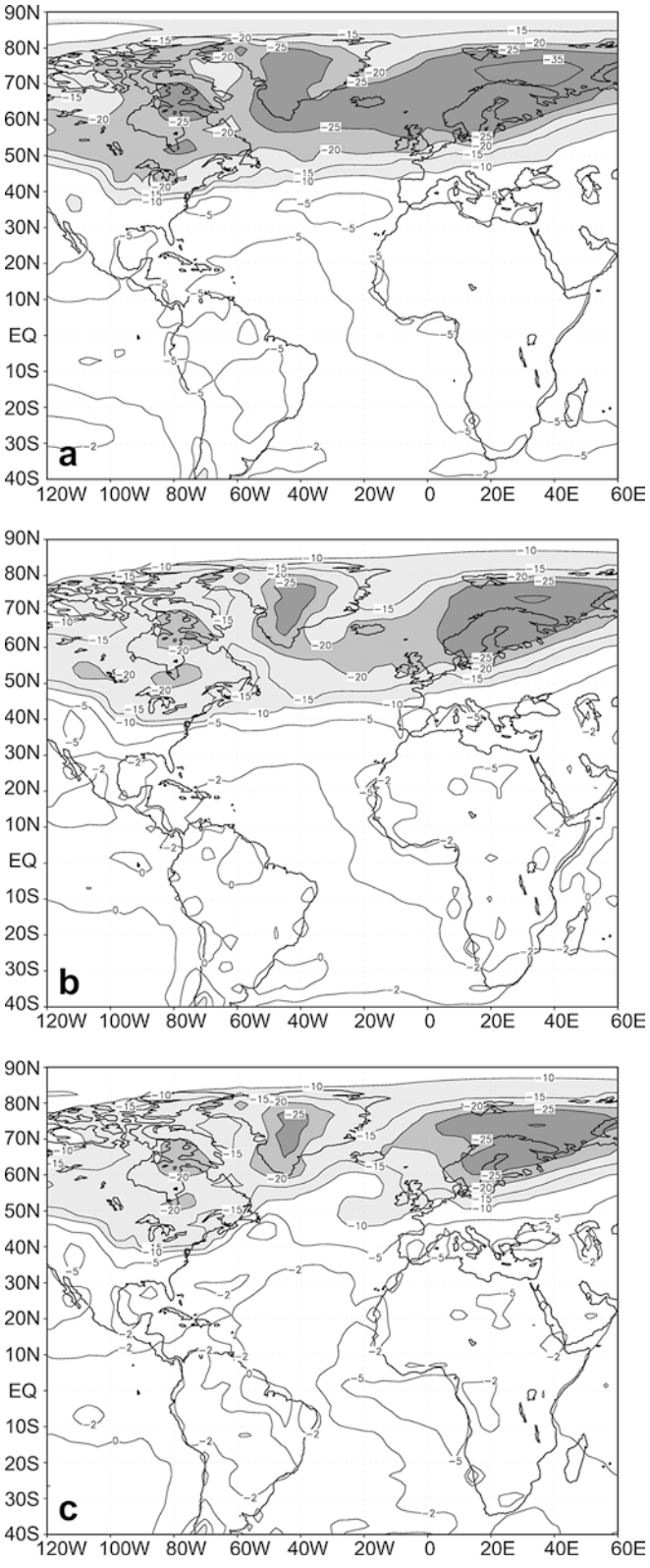

Fig. 1 Differences between the glacial and present-day annual mean air temperatures for different reconstructions: **a** CLIMAP (1981) with tropical cooling (Lohmann and Lorenz 2000), **b** Weinelt et al. (1996), **c**GLAMAP 2000 (Paul and Schaefer-Neth 2003)

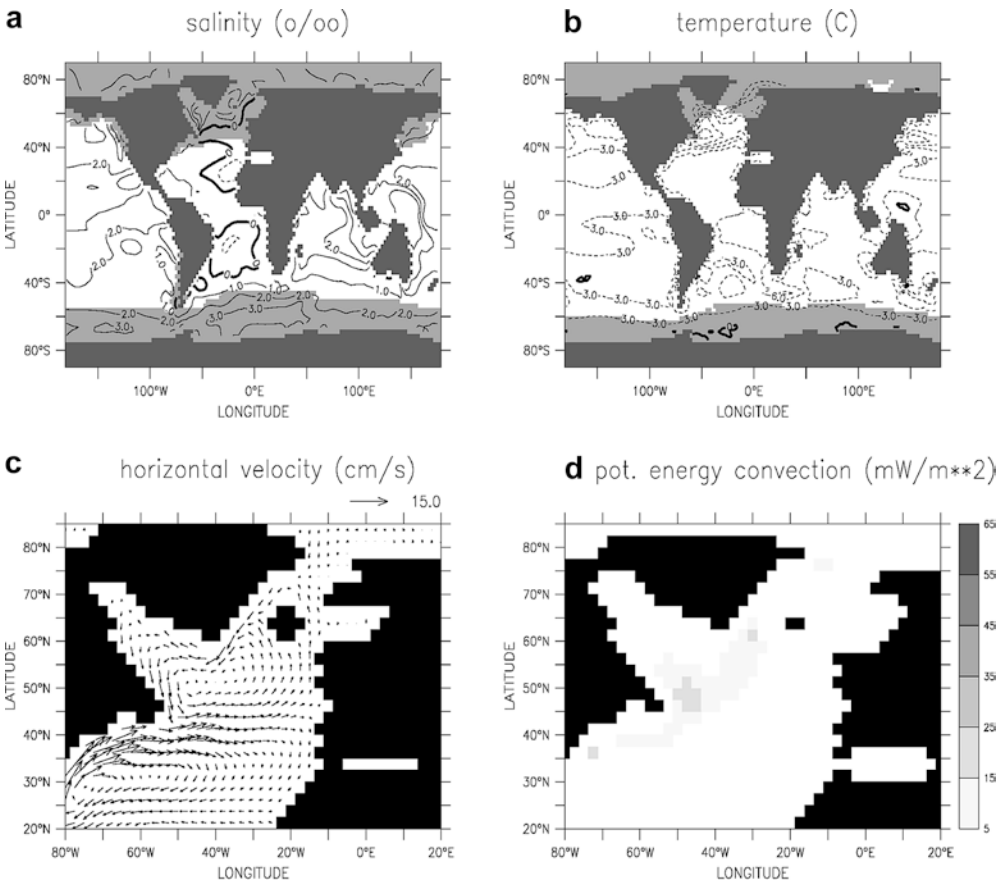

Fig. 2 Differences of the equilibrium states (as a 40 year mean) of experiment **C** and present-day for: **a** global salinity (contour interval 1.0 psu), the *shading* indicates the winter sea-ice cover; **b** global temperature (contour interval 3 °C), the *shading* indicates the summer sea-ice cover. **c** Absolute horizontal velocities; **d** the convection sites in the North Atlantic. Salinity, temperature and velocity fields are averaged over the top 150 m

37.0 psu), and an area of freshwater in the North Pacific (of around 33.0 psu). Therefore, it has formed a bipolar saline-fresh structure opposite to the Atlantic structure, a configuration similar to the present-day distribution. The salinity anomalies **W**–**C** and **G**–**C** (Figs. 3a and 4a) show fresher conditions in the Pacific. The model simulates an Indonesian salinity maximum in the Indian Ocean and the Western Pacific.

Figure 2b shows annual mean temperature anomalies relative to present-day values, averaged over the uppermost 150 m, for experiment **C**. Very strong temperature gradients (not shown) are located in the Atlantic between 35°N and 55°N. The temperature front, which is zonal in **C** (Fig. 2b), is turned to a more meridional direction in experiment **W** (Fig. 3b) and **G** (Fig. 4b). Strong anomalies are found near Newfoundland (up to 10 °C) in experiment **G**.

In all three experiments, the subtropical and subpolar Atlantic gyres are well simulated (Figs. 2c, 3c and 4c). The warm North Atlantic Current divides into three parts. The first part flows into the Nordic Seas, circulating around Iceland and, after cooling, the waters head southward through the cold East Greenland Current. This horizontal circulation appears to be stronger for **G** and **W**. The second part of North Atlantic waters is advected southwards, to the eastern branch of the subtropical gyre. The third part of the current system circulates cyclonically in the latitudes south of Iceland forming the subpolar gyre. The last type of circulation is particularly strong in **C**. In conclusion the horizontal circulation for the climates with warm glacial conditions appear more meridionally than in experiment **C**.

The North Atlantic convection sites (Figs. 2d, 3d and 4d) in the glacial simulations are located near the North American coast, in the Labrador Sea and in the Irminger Sea. The convective areas are between 40°N and 65°N in all cases. This differs from the present-day pattern, simulated with the same model, where the regions of convection are situated mainly in the Nordic Seas and in the Labrador Sea (Prange et al. 2003). The southward displacement of the convection sites in the glacial simulations is associated with a southward shift of NADW formation. In spite of this common general feature, the three experiments differ in convection strength and geographical details in the convective patterns. Convective activity is strongest in experiment **G** and weakest in experiment **C**. Investigating the seasonality of the convection, the maximum activity in **C** is found in autumn, when the temperatures of the surface waters are low enough to form denser waters for convection to start. The required cooling for maximum convection occurs in the early autumn, rather than in winter, due to the low summer temperatures. In experiment **G**, maximum convection occurs in January, several months later than in **C**, as a result of the longer time for the necessary surface water cooling. In experiment **W**, the

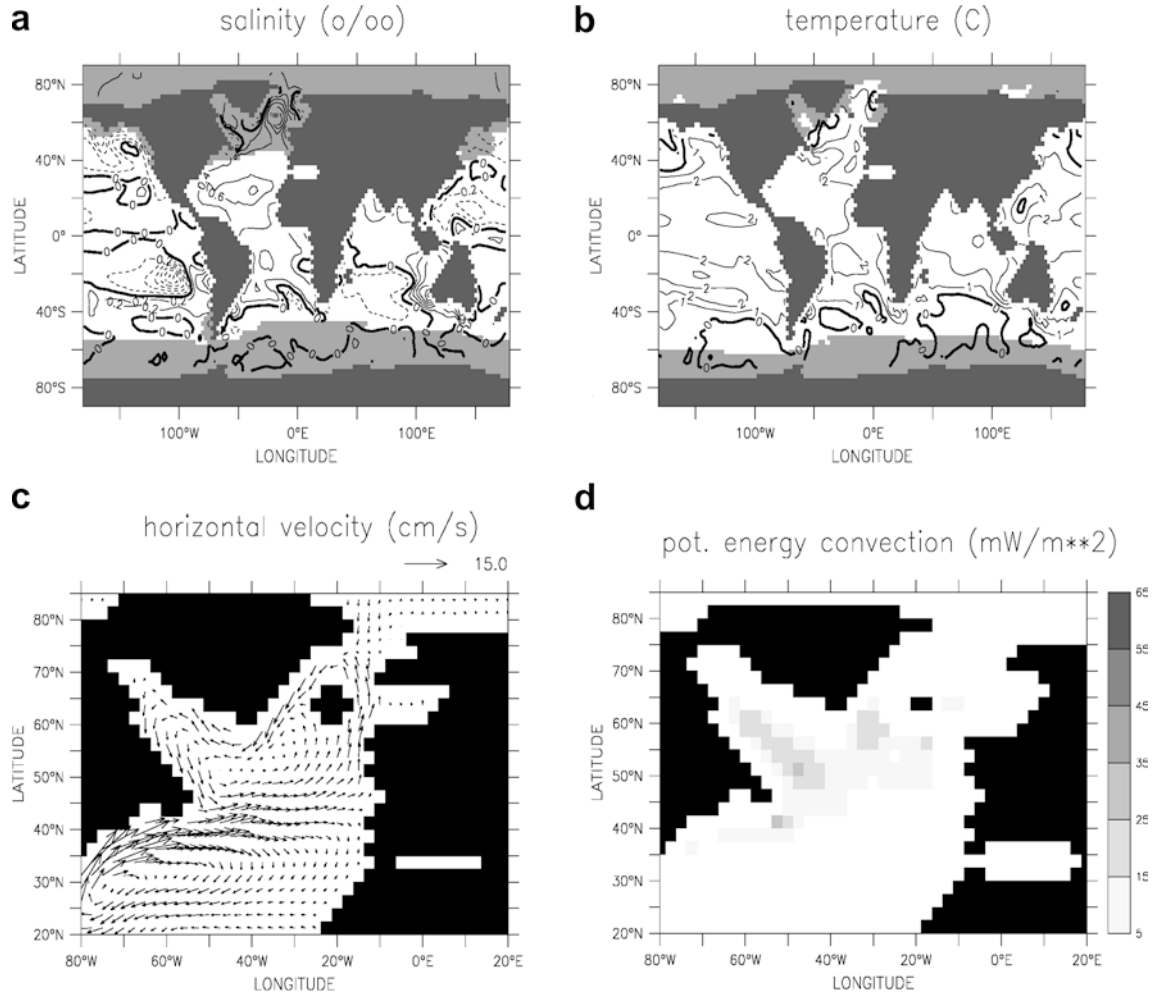

Fig. 3 As in Fig. 2, differences between experiments **W** and **C**. The contour intervals for **a** are 0.2 psu and for **b** are 1 °C

maximum convection is found in late autumn, as the summer surface waters are warmer than in **C**, but cooler than in **G**.

Experiment **C** yields a North Atlantic overturning cell down to 2500 m (Fig. 5a). The net NADW export at 30°S amounts to 7 Sv (1 Sv = 10^6 m^3 s^{-1}). The maximum North Atlantic meridional overturning is 12 Sv. Below 3500 m, AABW (Antarctic Bottom Water) enters the Atlantic with a volume flux of 3 Sv. In experiment **W**, the North Atlantic overturning cell is much deeper, occupying almost the whole Atlantic basin. The maximum overturning is 20 Sv and the net export of NADW at 30°S is about 15 Sv. In experiment **G** the meridional overturning is even stronger (more than 20 Sv) with a greater export at 30°S (around 16 Sv). The values of maximum North Atlantic overturning in both experiments **G** and **W** are about 70% greater than in experiment **C**. Moreover, the meridional heat transport into the Atlantic basin also differs significantly for the three experiments. Its maximum is found in all experiments around 30°N with values of 0.83 PW, 1.23 PW and 1.42 PW for experiments **C**, **W** and **G**, respectively.

3.3 Atlantic freshwater budgets and hystereses

To assess the role of the hydrological balance for the stability of the THC, we integrated the surface freshwater fluxes over the Atlantic Ocean (including the Arctic). The calculations reveal a net freshwater loss for the ocean in all three experiments (Fig. 6), i.e. a predominant evaporative regime. The lowest value of the balancing oceanic freshwater import at 30°S is found in experiment **C** and the highest value in experiment **G**. A plot of the zonal mean precipitation (P), evaporation (E) and P–E over the Atlantic basin for the three experiments is shown in Fig. 7. The precipitation follows a similar structure in all experiments (Fig. 7a), maximum in the tropical and mid-latitude regions and minimum in the subtropical and polar latitudes, as the values increase from experiments **C** to **W** and **G**. The evaporation rates are at a maximum between 30°S and 30°N and are highest for the warmer climates (Fig. 7b). Enhanced evaporation is also found in the northern mid-latitudes for experiment **W** and even more pronounced for experiment **G**, due to the ice-free Nordic Seas and warmer conditions in this region. A weaker hydrological

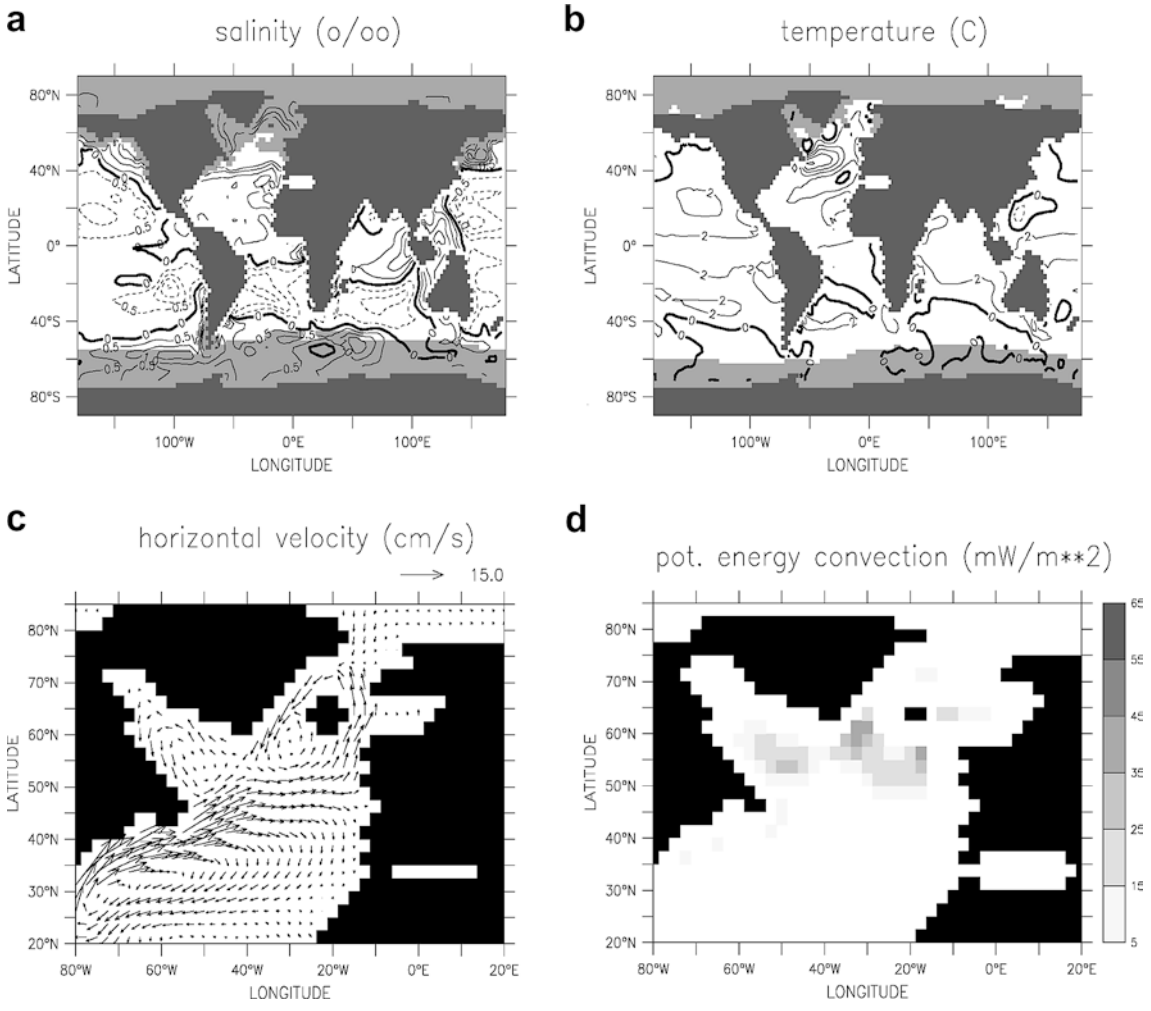

Fig. 4 As in Fig. 2, differences between experiments **G** and **C**. The contour intervals for **a** are 0.5 psu and for **b** are 2 °C

cycle is found in experiment **C** compared with **W** and **G**. The main difference between the hydrology in the experiments appears in the tropical and subtropical latitudes (Fig. 7c). The differences in spatial patterns of the surface freshwater flux ($P - E$) between experiments **G** and **W** and the experiment **C**, are shown in Fig. 8. In subequatorial and tropical latitudes, anomalous negative freshwater fluxes (experiment **C** refers to the experiment LGM.N in Lohmann and Lorenz 2000) are associated with large water vapour transport from the Atlantic to the Pacific. The same general trends are found in the **G** and **W** simulations, as the strengths of the negative centres are stronger in the same tropical areas. Positive anomalies relative to **C** are situated along the thermal equator and in mid-latitudes. Thus the three different experiments provide for three different hydrological cycles. The contribution of the overturning component of the Atlantic freshwater transport is calculated through: $F_{ot} = -\frac{1}{S_0}\int \bar{v}\bar{S}\,\mathrm{d}z$ (Prange et al. 2003; Lohmann 2003). The integral is calculated over the depth, $\bar{S}$is the zonally averaged salinity, $\bar{v}$is the zonally integrated meridional velocity and $S_0 = 35$ psu is a reference salinity. At 30°S, the lowest value of the freshwater transport due to the overturning is found in experiment **C** ($F_{ot} = 0.034$ Sv), followed by experiment **W** ($F_{ot} = 0.054$ Sv), and the largest value is found in experiment **G** ($F_{ot} = 0.072$ Sv). When comparing these numbers with the total freshwater loss, it is concluded that the overturning component of the freshwater transport is only a minor part of the net evaporation over the Atlantic.

Aiming to find a link between hydrology and stability of the glacial THC, we calculate hysteresis stability diagrams. A slowly varying freshwater flux perturbation (10^{-4} Sv/year) is applied to the North Atlantic between 20°N and 50°N. The sequence of quasi-equilibrium states is reflected by the upper branch of the hysteresis, down to the 'critical point' where the freshwater input causes a complete shutdown of the THC. Then the freshwater input is decreased so that the circulation recovers. Afterwards, the freshwater input is increased again in order to return to the initial state. The resulting hysteresis diagrams for experiments **C**, **W** and **G** are displayed in Fig. 9. In experiment **C**, an anomalous ('critical') freshwater flux of 0.16 Sv is required for a THC shutdown. The 'critical' freshwater input increases

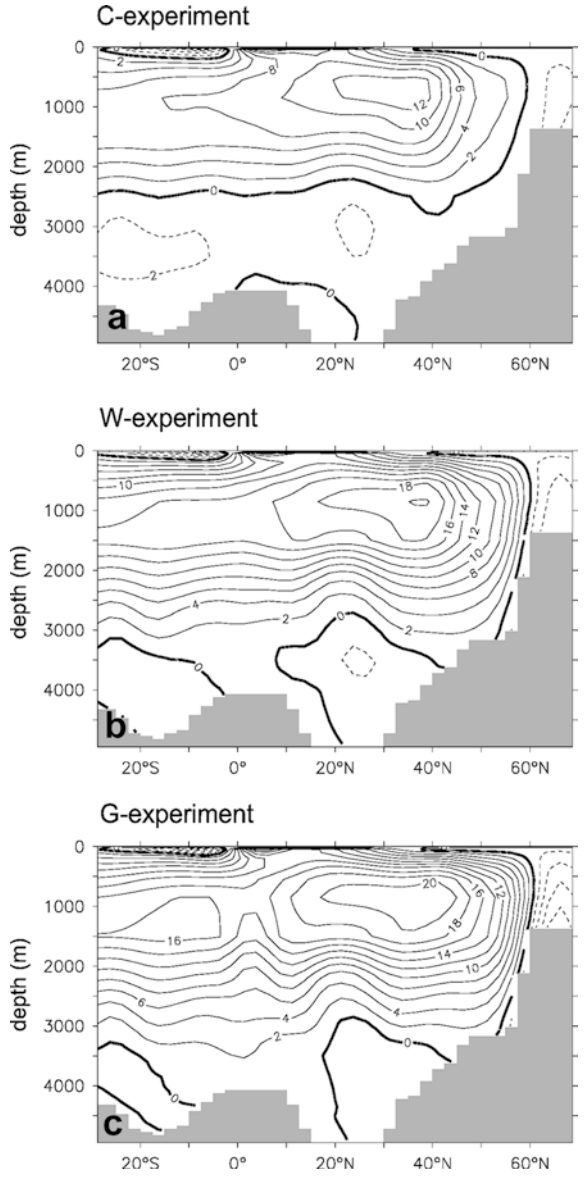

Fig. 5 Atlantic meridional overturning streamfunction in Sv for experiments **a C**, **b W** and **c G**. All panels represent a 40 year mean

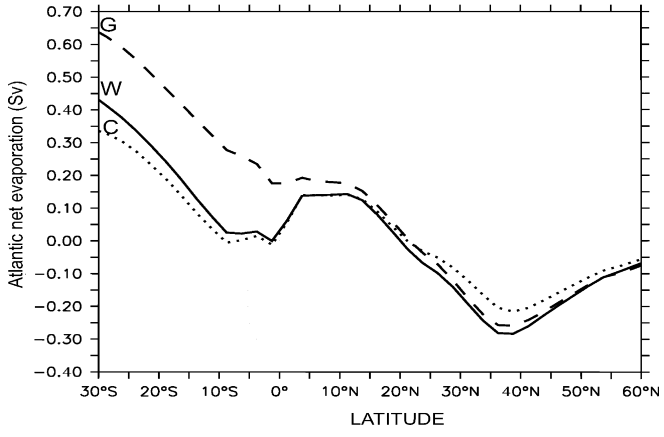

Fig. 6 Northward freshwater transport in the Atlantic for experiments **C**, **W** and **G**

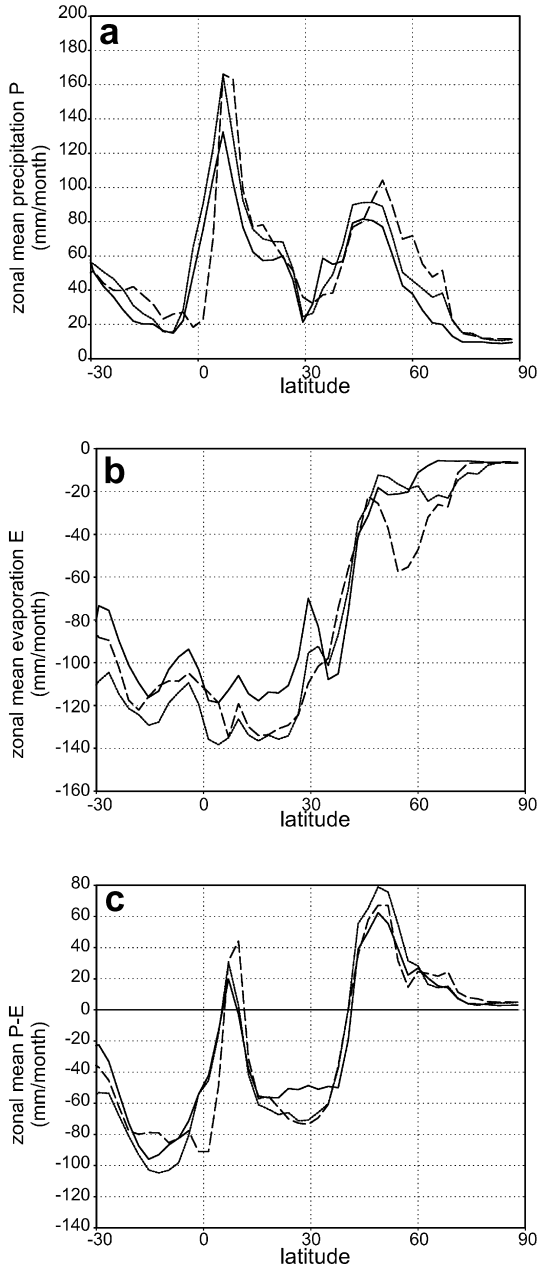

Fig. 7 **a** Zonal mean precipitation *P*, **b** zonal mean evaporation *E*, and **c** zonal mean *P–E* over the Atlantic basin for experiments **C** (*solid line*), **W** (*short dashed line*) and **G** (*long dashed line*). The units are mm/month

for **W** and **G** (0.24 Sv and 0.36 Sv, respectively). In Fig. 10 the dependence of the 'critical' freshwater perturbation on the net evaporation rate is displayed. The graph suggests a monotonic relationship between the stability of the ocean circulation and the hydrological budget in the Atlantic Ocean.

4 Discussion

One could pose the question whether the glacial THC was weaker than the present-day circulation. In our cold

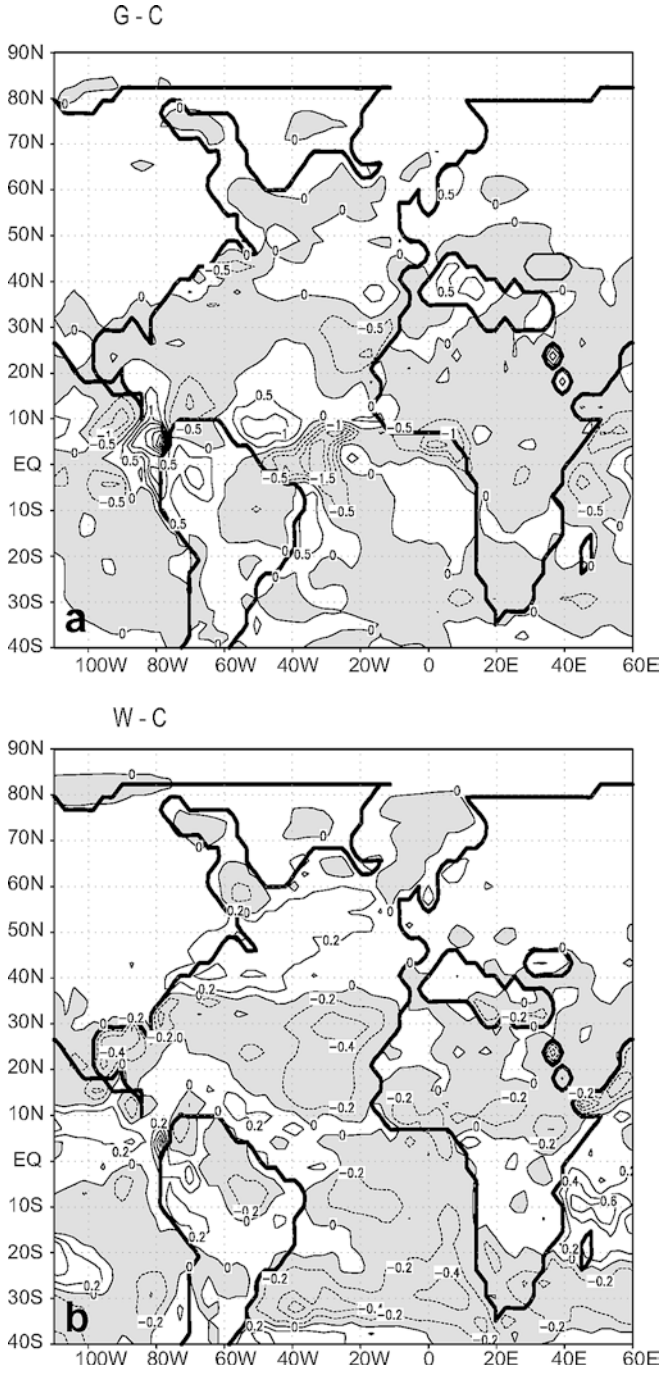

Fig. 8 Surface freshwater flux ($P - E$) differences in the Atlantic area: **a** between **G** and **C**; **b** between **W**and **C**. The *grey fill* shows the areas of negative anomalies. Units are m/year

glacial simulation (experiment **C**) we find a reduction of 20% of the Atlantic meridional overturning circulation relative to the present-day simulation (Prange et al. 2003). Utilizing different kinds of coupled models, Weaver et al. (1998), Ganopolski and Rahmstorf (2001), and Shin et al. (2003) simulated a similar weakening of the conveyor during the glacial maximum, which is consistent with the geological findings of Rutberg et al. (2000), who, based on ratios of neodymium isotopes,

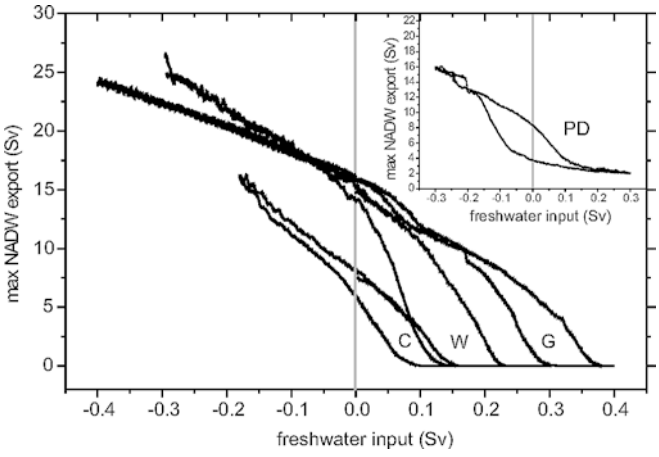

Fig. 9 The hysteresis loops for the experiments **C**, **W** and **G**. The equilibrium states of the experiments **C**, **W** and **G** are situated on the *zero line* of the freshwater input. In the *upper right corner* of the plot the present-day (control run) hysteresis is shown (Prange et al. 2002)

reported weakening of NADW export to the Southern Ocean during the full glacial stages (e.g. LGM), and almost no change during the warm glacial intervals. A weaker circulation is also consistent with assimilated paleonutrient tracer distribution in an ocean circulation model (Winguth et al. 1999). Furthermore, benthic foraminifera δ^{13}C, Cd/Ca and Ba/Ca ratios suggest that the deep Atlantic circulation during the LGM was influenced by the deep penetration of AABW and consequent reduction of NADW (Boyle and Keigwin 1987; Duplessy et al. 1988; Boyle 1992; Marchitto et al. 2002). A shallower overturning cell, approximately 1000 m less than present-day, is also indicated by the shoaling of the sedimentary lysocline, which gives the interface between NADW and AABW (Volbers and Henrich 2003, Frenz and Henrich submitted 2003). However, the strength of the overturning remains a controversial topic. No change of the overturning rate is inferred from sedimentary records of ^{231}Pa/^{230}Th (Yu et al. 1996) and a new reconstruction combining 55 benthic foraminiferal stable carbon isotopes suggests no considerable difference

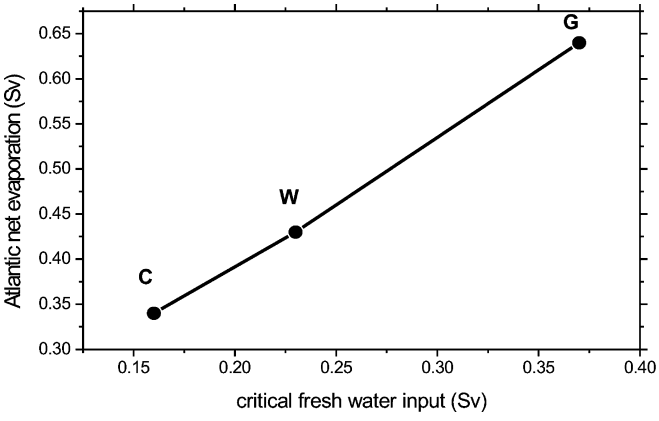

Fig. 10 The freshwater export at 30°S versus the 'critical' freshwater input for reaching the 'off-mode'

to the present-day circulation strength (Bickert and Mackensen 2003). On the other hand, three-dimensional coupled models even resulted in intensification of the LGM ocean circulation (Hewitt et al. 2001; Kitoh et al. 2001). Our simulations with warm glacial background conditions (**W** and **G**) also exhibit stronger (around 50%) overturning compared to the present-day simulation in Prange et al. (2003).

Using different SST reconstructions, we are able to detect different glacial salinity distributions at the surface and in the depth. In experiment **C**, the SSS field shows a tongue of salty waters deeply penetrating from the subtropics to the southern vicinities of Iceland, a feature consistent with the reconstructions of Duplessy et al. (1991). For warm background conditions (**W** and **G**) a salinity increase in the Irminger Sea is responsible for the stronger convection and NADW formation. The modelled salinities in the North Atlantic are more consistent with the reconstructions of Duplessy et al. (1991) for both types of experiments with warm (**W** and **G**) and cold (**C**) conditions, and they differ substantially (by more than 1.5 psu) from the values suggested by de Vernal et al. (2000). The mean surface salinity of the glacial ocean appears relatively fresh compared to the present one in our model. The salinity excess of the glacial ocean ($+1$ psu) is mainly stored in the abyssal ocean, consistent with geological evidence (Adkins et al. 2002).

All experiments for the glacial ocean yield an Atlantic Ocean saltier than the Pacific, similar to the present-day configuration. However, the model study of Lautenschlager et al. (1992) finds the opposite contrast with the Pacific Ocean being saltier than the Atlantic. The simulations of the present-day climate with reduced greenhouse gases, performed by Shin et al. (2003), show also the opposite contrast, but their coupled LGM simulation reveals a fresher Pacific and a saltier Atlantic Ocean relative to present day. An intensification of the salinity contrast between the Atlantic and Pacific oceans is found in experiments **G** and **W** relative to **C**, which originates from strongly increased moisture export out of the Atlantic to the Pacific Ocean. In experiment **C**, Lohmann and Lorenz (2000) attributed this to enhanced water vapour transport over Panama, reduced water input over the dry African continent and a smaller water vapour import over the North American continent. The latter effect is linked to the presence of the large continental ice-sheets.

Perturbations of the glacial THC with different climatic background states result in different hysteresis maps. At zero freshwater input, the glacial THC has one stable equilibrium only. This can be directly inferred from the hysteresis curves for experiments **W** and **G** (Fig. 9). The weak bistability at zero freshwater input in experiment **C** is caused by the relative high freshwater flux perturbation rate of 10^{-4} Sv/year compared to our previous work where we found a strict monostability at the zero point (Prange et al. 2002). In each experiment, the freshwater budget reveals a net evaporation over the Atlantic (including Arctic) catchment area with different strengths. The experiments show that higher net evaporation tends to shift the equilibrium to a more stable state. The hystereses show that the coldest climate is more sensitive to freshwater changes than the warm glacial climates. The salinity enhancement along the conveyor route through the subtropics induces a northward freshwater transport across 30°S compensating the freshwater loss from the evaporation. It may be split into an overturning component, a component related to the gyre circulation, and a term related to diffusion. The small values, which are found for the overturning component, suggest that gyre and diffusive transports play an important role for the stability of the THC. Consistent with Saenko et al. (2002), F_{ot} is a poor measure for the stability of the conveyor. During glacial times, the salinity and temperature induced density gradients between the North and South Atlantic act in one direction driving the conveyor, which corresponds to the thermo-haline regime of the ocean system according to Rahmstorf's (1996) definition. The strong salinity contrast between the South Atlantic and the North Atlantic in experiment **G** is associated with a stronger haline-driven ocean circulation. The haline factor is weaker in experiment **W**, which is partly compensated by the thermal forcing. The predomination of the haline mechanism induces a stabilizing effect on the THC, which allows only one stable state of the circulation, namely an on-mode with NADW formation.

We relate the 'critical' freshwater input, which causes the collapse of the circulation, to the hydrological background conditions. The lower evaporation rates over the Atlantic basin in the cold glacial climate of experiment **C** results in a less stable circulation, while the warmer climates with higher Atlantic net evaporation are more stable. In this sense, the stability parameters depend explicitly on the background hydrology with a monotonic (almost linear) relation between the Atlantic evaporation rates and the 'critical' perturbation.

The glacial THCs substantially differ from the present-day circulation. Using present-day forcing, our model produces a THC with two stable equilibria (Prange et al. 2003), like many other models. Freshwater perturbations can shut down the overturning irrevocably. In the present-day ocean, the THC is driven by SST gradients, while salinity gradients across the Atlantic Ocean tend to weaken the overturning, which allows multiple equilibria of the ocean circulation in the thermal flow regime (Stommel 1961; Rahmstorf 1996). In a coupled three-dimensional OGCM with an energy-moisture balance model for the atmosphere including an ice sheet component, the glacial THC possesses different stability properties (Schmittner et al. 2002). As the ice sheet component in this model set-up does not permit the system to settle into equilibrium, this glacial ocean is characterized by a mode different than the one studied here. In the absence of anomalous freshwater fluxes, their experiments showed only one stable glacial mode, namely the off-mode.

5 Conclusions

In this study we performed three glacial simulations using three different reconstructions of SST and sea-ice margin as forcing fields for an AGCM. One reconstruction, based on CLIMAP (1981) with additional tropical cooling generates a cold glacial climate equilibrium, whereas the Weinelt et al. (1996) and GLAMAP 2000 (Paul and Schäfer-Neth 2003) reconstructions produce relatively warm glacial climate backgrounds in the North Atlantic realm. In contrast to the present-day THC, all equilibrium states of the simulated LGM climates show a mono-stable behaviour, which can serve as an explanation for the recovery of the THC after meltwater-induced shutdowns (Ganopolski and Rahmstorf 2001; Prange et al. 2002).

In the differing glacial climate backgrounds, the warm climates show higher stability than the cold climate. By analyzing the hydrological balance in the Atlantic catchment area, we find a monotonic dependence between the Atlantic net evaporation and the 'critical' freshwater input in the hysteresis causing a complete collapse of the THC. We conclude that the background hydrological balance plays a crucial role for the stability of the ocean circulation and, hence, of the glacial climate. Since THC changes sensitively depend on the climatic background state with its associated hydrological cycle, our modelling strategy, employing an AGCM in T42 resolution with explicitly resolved hydrological cycle seems to be appropriate. This suggests an important role of the low-latitude hydrological cycle for the branching and sensitivity of the THC. Such a hydrological bridge and its changes have been attributed to changes of interannual variability in the tropical Pacific Ocean (Latif et al. 2000; Schmittner and Clement 2002) as well as to times of weak overturning causing enhanced water vapour transport over the Isthmus of Panama (Lohmann 2003). Moreover, changes in the South Atlantic, connected with the cold and warm water routes of the global ocean circulation (Gordon 1986) may strongly determine the regime of the THC (Knorr and Lohmann 2003).

In our model set-up, we have neglected feedbacks connected with atmosphere dynamics, vegetation and the cryosphere. Changes in the hydrological balance are estimated to be in the order of 0.15 Sv, when comparing the climate state of the on and off mode in a coupled atmosphere–ocean general circulation model (Lohmann 2003). The cryosphere provides a great uncertainty. Iceberg discharge has been estimated to be of order 0.15 Sv for 500–1000 years (Calov et al. 2002; Chappell 2002). The effect of vegetation cover on the interocean basin water vapour transport has not been analyzed so far.

In this study, we have not addressed the extent to which the climatic templates represent real glacial climate states. One could speculate that the modelled THC states may possess features of stadial and interstadial circulations, respectively. The different hydrological budgets during relatively cold and warm background conditions would then imply different sensitivities with respect to Heinrich Events (cold conditions) and the Younger Dryas (about 13,000-11,500 years BP), a cold phase which directly followed the warm Bølling-Allerød period. Our study emphasizes the importance of the tropical hydrological cycle, which may provide a possible link between the low latitudes and the ocean circulation on paleoclimatic time scales. In order to understand these linkages, more geological data for the tropical regions is required.

Acknowledgements We gratefully acknowledge the comments and suggestions of Andre Paul, Christian Schäfer-Neth and Klaus Grosfeld, and Andreas Manschke and Silke Schubert for technical support. We also thank the reviewers for constructive comments. The study was funded by the BMBF through DEKLIM project Climate transitions and by the Deutsche Forschungsgemeinschaft as a part of the DFG Research Centre 'Ocean Margins' of the University of Bremen (No. RCOMO127).

References

Adkins JF, McIntyre K, Schrag DP (2002) The salinity, temperature and $\delta^{18}O$ content of the glacial deep ocean. Science 298: 1769–1773

Bickert T, Mackensen A (2003) Last Glacial to Holocene Changes in South Atlantic deep water circulation. In: The South Atlantic in the Quaternary Reconstruction of material budget and current systems. Wefer G, Mulitza S, Rathmeyer V, . Springer, Berlin Heidelberg, pp 599–620

Boyle EA (1992) Cadmium and $\delta^{13}C$ paleochemical ocean distribution during the stage 2 glacial maximum. Ann Rev Earth Planet Sci 20: 245–287

Boyle EA, Keigwin LD (1987) North Atlantic thermohaline circulation during the past 20,000 years linked to high-latitude surface temperature. Nature 330: 35–40

Broecker WS, Hemming S (2001) Climate swings come into focus. Science 294: 2308–2309

Bryan F (1986) High-latitude salinity effects and interhemispheric thermohaline circulations. Nature 323: 301–304

Calov R, Ganopolski A, Petoukhov V, Claussen M, Greve R (2002) Large-scale instabilities of the Laurentide ice sheet simulated in a fully coupled climate-system model. Geophys Res Let 29: 2216, doi:10.1029/2002GL016078

Chappell J (2002) Sea level changes forced ice breakouts in the Last Glacial cycle: new results from coral terraces. Quat Sci Rev 21: 1229–1240

Clark PU, Pisias NG, Stocker TF, Weaver AJ (2002) The role of the thermohaline circulation in abrupt climate change. Nature 415: 863–869

CLIMAP project members (1981) Seasonal reconstructions of the Earth surface at the Last Glaial Maximum. Geological Society of America Map and Chart Series, MC-36, 18 maps, Boulder, Colorado, USA

de Vernal A, Hillaire-Marcel C (2000) Sea-ice cover, sea-surface salinity and halo-/thermocline structure of the northwest North Atlantic: modern versus full glacial conditions. Quat Sci Rev 19: 65–68

Duplessy JC, Shackelton NJ, Fairbanks RG, Labeyrie L, Oppo D, Kallel N (1988) Deepwater source variations during the last climatic cycle and their impact on the global deepwater circulation. Paleoceanography 3: 343–360

Duplessy JC, Labeyrie L, Juillet-Leclerc A, Maitre F, Duprat J, Sarnthein M (1991) Surface salinity reconstruction of the North Atlantic Ocean during the last glacial maximum. Oceanologica Acta 14: 311–324

Fanning AF, Weaver AJ (1997) Temporal-geographical meltwater influences on the North Atlantic conveyor: implications for the Younger Dryas. Paleoceanography 12: 307–320

Farrera I, Harrison SP, Prentice IC, Ramstein G, Guiot J, Bartlein PJ, Bonnefille R, Bush M, Cramer W, von Grafenstein U, Holmgren K, Hooghiemstra H, Hope G, Jolly D, Lauritzen SE, Ono Y, Pinot S, Stute M, Yu G (1999) Tropical climates at the Last Glacial Maximum: a new synthesis of terrestrial paleoclimate data. I. Vegetation, lake-levels and geochemistry. Clim Dyn 15: 823–856

Ganopolski A, Rahmstorf S (2001) Simulation of rapid glacial climate change in a coupled climate model. Nature 409: 153–158

Gordon AL (1986) Interocean exchange of thermocline water. J Geophys Res 91: 5037–5046

Hewitt CD, Broccoli AJ, Mitchell JFB, Stouffer RJ (2001) A coupled model study of the last glacial maximum: was part of the North Atlantic relatively warm? Geophys Res Lett 28: 1571–1574

Kitoh A, Murakami FS, Koide H (2001) A simulation of the Last Glacial Maximum with a coupled atmosphere-ocean GCM. Geophys Res Lett 28: 2221–2224

Knorr G, Lohmann G (2003) Southern Ocean origin for resumption of Atlantic thermohaline circulation during deglaciation. Nature 424: 532–536

Latif M, Roeckner E, Mikolajewicz, Voss R (2000) Tropical stabilization of the thermohaline circulation in a Greenhouse warming simulation. J Clim 13: 1809–1813

Lautenschlager M, Mikolajewicz U, Maier-Reimer E, Heinze C (1992) Application of ocean models for the interpretation of the atmospheric general circulation model experiments on the climate of the Last Glacial Maximum. Paleoceanography 7: 769–782

Leonard BP (1979) A stable and accurate convective modelling procedure based on quadratic upstraem interpolation. Comput Meth Appl Mech Eng 19: 59–98

Lohmann G (2003) Atmospheric and oceanic freshwater transport during weak Atlantic overturning circulation. Tellus 55A: 438–449

Lohmann G, Lorenz S (2000) On the hydrological cycle under paleoclimatic conditions as derived from AGCM simulations. J Geophys Res 105: 17,417–17,436

Lohmann G, Gerdes R, Chen D (1996a) Sensitivity of the thermohaline circulation in coupled oceanic GCM-atmospheric EBM experiments. Clim Dyn 12: 403–416

Lohmann G, Gerdes R, Chen D (1996b) Stability of the thermohaline circulation in a simple coupled model. Tellus 48A: 465–476

Maier-Reimer E, Mikolajewicz U (1989) Experiments with an OGCM on the cause of the Younger Dryas. Tech. Rep. 39, Max-Planck-Inst for Meteorol, Hamburg, pp 13

Maier-Reimer E, Mikolajewicz U, Hasselmann K (1993) Mean circulation of the Hamburg LSG OGCM and its sensitivity to the thermohaline surface forcing. J Phys Oceanogr 23: 731–757

Manabe S, Stouffer RJ (1995) Simulation of abrupt climate change induced by freshwater input to the North Atlantic Ocean. Nature 378: 165–167

Marchitto TM, Oppo DW, Curry WB (2002) Paired benthic foraminiferal Cd/Ca and Zn/Ca evidence for a greatly increased presence of Southern Ocean Water in the glacial North Atlantic. Paleoceanography 17: 1038, doi:10.1029/2000PA000PA000598

Mikolajewicz U, Maier-Reimer E (1994) Mixed boundary conditions in ocean general circulation models and their influence on the stability of the model's conveyor belt. J Geophys Res 99: 22,633–22,644

Mix AC, Bard E, Schneider R (2001) Environmental processes of the Ice Age: land, ocean, glaciers (EPILOG). Quat Sci Rev 20: 627–657

Paul A, Schäfer-Neth C (2003) Modeling the water masses of the Atlantic Ocean at the Last Glacial Maximum. Paleoceanography 18(3): 1058, doi:10.1029/2002PA000783

Peltier WR (1994) Ice age paleotopography. Science 265: 195–201

Prange M, Lohmann G, Gerdes R (1997) Sensitivity of the thermohaline circulation for different climates – investigations with a simple atmosphere-ocean model. Palaeoclimates 2: 71–99

Prange M, Romanova V, Lohmann G (2002) The glacial thermohaline circulation: stable or unstable? Geophys Res Lett 29: 2028, doi:10.1029/2002GL015337

Prange M, Lohmann G, Romanova V, Butzin M (2004) Modelling tempo-spatial signatures of Heinrich Events: influence of the climatic background state. Quat Sci Rev 23:521–527

Prange M, Lohmann G, Paul A (2003) Influence of vertical mixing on the thermohaline hysteresis: analyses of an OGCM. J Phys Oceanogr 33: 1707–1721

Rahmstorf S (1995) Bifurcations of the Atlantic thermohaline circulation in response to changes in the hydrological cycle. Nature 378: 145–149

Rahmstorf S (1996) On the freshwater forcing and transport of the Atlantic thermohaline circulation. Clim Dyn 12: 799–811

Rahmstorf S, Willebrand J (1995) The role of temperature feedback in stabilizing the thermohaline circulation. J Phys Oceanogr 25: 787–805

Rind D, deMenocal P, Russell G, Sheth S, Collins D, Schmidt GA, Teller J (2001) Effects of glacial meltwater in the GISS coupled atmosphere-ocean model: Part I: North Atlantic Deep Water response. J Geophys Res 106: 27,335–27,354

Roeckner E, Arpe K, Bengtsson L, Brinkop S, Dümenil L, Esch M, Kirk E, Lunkeit F, Ponater M, Rockel B, Sausen R, Schlese U, Schubert S, Windelband M (1992) Simulation of the present-day climate with ECHAM model: impact of model physics and resolution, S. 28, Hamburg, Germany, pp 171

Rühlemann C, Mulitza S, Lohmann G, Paul A, Prange M, Wefer G (2004) Intermediate-depth warming in the tropical Atlantic related to weakened thermohaline circulation: combining paleoclimate and modeling data for the last deglaciation. Paleoceanography 19. Doi:1029/2003PA0000948

Rutberg RL, Hemming SR, Goldstein SL (2000) Reduced North Atlantic Deep Water flux to the glacial Southern Ocean inferred from neodymium isotope ratios. Nature 405: 935–938

Saenko O, Gregory JM, Weaver AJ, Eby M (2002) Distinguishing the influence of heat, freshwater, and momentum fluxes on ocean circulation and climate. Clim Dyn 15: 3686–3697

Sarnthein M, Gersonde R, Niebler S, Pflaumann U, Spielhagen R, Thiede J, Wefer G, Weinelt M (2003) Overview of Glacial Atlantic Ocean Mapping (GLAMAP 2000). Paleoceanography 18: 1030, doi:10.1029/2002PA000769

Schäfer-Neth C, Paul A (2001) Circulation of the glacial Atlantic: a synthesis of global and regional modeling. In: The Northern North Atlantic: A Changing Environment. Schäfer IP, Ritzrau W, Schlüter M, Thiede J, Springer, Berlin, pp 446–462

Schiller A, Mikolajewicz U, Voss R (1997) The stability of the North Atlantic thermohaline circulation in a coupled ocean-atmosphere general circulation model. Clim Dyn 13: 325–347

Schmittner A, Clement AC (2002) Sensitivity of the thermohaline circulation to tropical and high latitude freshwater forcing during the last glacial-interglacial cycle. Paleoceanography 17: 10.1029/2000PA000591

Schmittner A, Yoshimori M, Weaver AJ (2002) Instability of glacial climate in a model of ocean-atmosphere-cryosphere system. Science 295: 1489–1493

Shin S, Liu Z, Otto-Bliesner BL, Brady EC, Kutzbach JE, Harrison SP (2003) A simulation of the Last Glacial Maximum climate using the NCAR-CCSM. Clim Dyn 20: 127–151

Stocker TF, Wright DG (1991) Rapid transitions of the ocean's deep circulation induced by changes in surface water fluxes. Nature 351: 729–732

Stommel H (1961) Thermohaline convection with two stable regimes of flow. Tellus 13: 224–230

Volbers ANA, Henrich R (2002) Present water mass calcium carbonate corrosiveness in the eastern South Atlantic inferred from ultrastructural breakdown of Globigerina bulloides in surface sediments. Marine Geology 186:471–486

Weaver AJ, Eby M, Fanning AF, Wiebe EC (1998) Simulated influence of carbon dioxide, orbital forcing and ice sheets on the climate of the Last Glacial Maximum. Nature 394: 847–853

Weinelt M, Sarnthein M, Pflaumann U, Schulz H, Jung S, Erlenkeuser H (1996) Ice-free Nordic Seas during the Last Glacial Maximum? Potential sites of deepwater formation. Palaeoclimates 1: 283–309

Winguth AME, Archer D, Maier-Reimer E, Mikolajewicz U, Duplessy JC (1999) Sensitivity of paleonutrient tracer distributions and deep-sea circulation to glacial boundary conditions. Palaeoceanography 14: 304–323

Yu EF, Francois R, Bacon MP (1996) Similar rates of modern and last glacial ocean thermohaline circulation inferred from radiochemical data. Nature 379: 689–694